Hindawi
Advances in Civil Engineering
Volume 2020, Article ID 4515319, 20 pages
https://doi.org/10.1155/2020/4515319

Research Article

Performance Analysis of Prefabricated Steel-Spring Floating-Slab Track and Its Application to Urban Express Rail Transit

Xudong Huang,[1] Ping Li,[2] Xinwei Luo,[2] Liang Ling,[3] Abdulmumin Ahmed Shuaibu,[1,4] and Zhiping Zeng[1]

[1]*School of Civil Engineering, Central South University, Changsha, China*
[2]*Guangzhou Metro Design and Research Institute Co., Ltd., Guangzhou, China*
[3]*State Key Laboratory of Traction Power, Southwest Jiaotong University, Chengdu, China*
[4]*Department of Civil Engineering, Facility of Engineering, Ahmadu Bello University, Zaria, Nigeria*

Correspondence should be addressed to Liang Ling; liangling@swjtu.edu.cn

Received 16 August 2019; Revised 7 January 2020; Accepted 21 January 2020; Published 19 March 2020

Academic Editor: Pier Paolo Rossi

The aim of the research is the design of prefabricated steel-spring floating-slab track to be applied in urban express rail transit systems. Using a developed vehicle-track dynamic-coupling equation for steel-spring floating-slab track, the effects of length, thickness, vertical damping, and use of side-mounted isolators on the floating-slab track were investigated experimentally using full-scale model and under different working conditions. The finding of the study revealed the following: (1) The prefabricated steel-spring floating-slab track can be applied to urban express rail transit, because it meets the requirements of high-speed transit while efficiently reducing noise. (2) The floating-slab track's stability slightly increases with the increase of its length and thickness. As thickness increases, vertical displacement of the rail increases slightly, and lateral stability increases, thereby slightly improving the vehicle's running stability. (3) When the intercity electric multiple-unit train travels along the prefabricated steel-spring floating-slab-track bed at different speeds, the wheel-axle lateral force, wheel-rail vertical force, the derailment coefficient, the wheel-weight reduction rate, and the lateral acceleration of the vehicle body are all less than the specified limits of Chinese code, thus fully meeting the safety requirements of train operation. (4) Appropriately increasing the vertical-support damping of the floating slab can improve the vehicle's vertical dynamic performance, reduce the vertical displacement of the rail, and lower the vibration response of the floating slab. (5) Adding side-mounted vibration isolators at the joint of the floating slab could greatly improve the stability of the floating slab itself and appropriately reduce the vehicle's vertical vibration response. Due to the optimization and establishment of relevant factors influencing the performance of prefabricated steel-string floating-slab track achieved in the study, the results obtained are particularly useful for setting safety, comfort, and stability requirements of the floating slab.

1. Introduction

In recent years, the rapid development of urban express rail transit has brought great convenience to people's travel and transportation [1]. Urban express rail transit is an emerging category of rail transit, which is a cross between railway and urban rail transit, and is mainly used to solve intercity traffic problems. The development of urban express rail transit provides a new model for urban residents to live in one city and work in a neighboring city, which is of great significance for optimizing urban patterns and alleviating traffic problems in dense urban areas. Thus, the urban express rail transit system came into being to optimize urban patterns, ease the traffic pressure in dense urban areas, and better address public-transportation challenges between city centers and suburbs or satellite communities and between key towns.

Owing to the tight use of urban land, urban express rail transit lines are commonly located very close to residence areas or even in tunnels below residents' gathering places or on viaduct structures, which are gradually adopted in large areas

[2]. Because of this close proximity, a serious problem to be addressed is environmental vibration due to the high speed of urban express rail transit (such as 160 km/h, the design speed of Guangzhou Rail Transits nos. 18 and 22) [3, 4].

The floating-slab track is a structure that can effectively reduce vibration and noise caused by vehicles on rails. The proposed steel-spring floating-slab track uses a prefabricated reinforced-concrete structure to form an integral track. A steel-spring isolator is used to elastically isolate the track slab from the foundation to form a mass-spring vibration-isolation system. Furthermore, a side-mounted vibration isolator is incorporated to constrain lateral displacement and vibration of the track slab. The advantages are that the steel-spring floating-slab track has better three-dimensional elasticity, less lateral displacement, good vibration-isolation performance, and easiness to maintain and replace [5, 6].

Many scholars have investigated the dynamic characteristics of floating-slab track under vehicle loads [7–13]. In 2009, Zhai et al. proposed a method to investigate the dynamics of vehicle-track systems with emphasis on theoretical modeling, numerical simulation, and experimental validation. They modeled a traditional ballasted track as two continuous parallel beams supported by a discrete elastic foundation consisting of three layers, including sleepers and ballasts. They also modeled the nonballasted slab track as two continuous parallel beams supported by a series of elastic rectangular slabs on a viscoelastic foundation [7]. On the basis of the above, a coupled-dynamics computation model for metro vehicles, and steel-spring floating-slab track, was developed as the influence of factors on the coupled system was explored such as the floating-slab dimensions (thickness and length) and mass, spring rate and spatial arrangement, and running speed [8]. MFM Hussein et al. proposed a new modeling method for discontinuous floating-slab track applied to subway. The coupling relationship between two submodels of track and tunnel under train load was expressed by Fourier series. The floating-slab track studied was found to display good vibration response [9]. Lombaert established a vehicle-track-foundation coupled dynamics model through three-dimensional numerical modeling method and evaluated the vibration reduction effect of the floating-slab track under different working conditions [10]. Hunt combined a vehicle with a track model to create a method that can be used to calculate the vibration transfer between the track and building. The results obtained in the study are valuable in evaluating the vibration response between rails, fasteners, floating track, and foundation [11]. Xu et al. proposed and applied a probabilistic model to simulate the characteristic of track irregularities by employing vehicle-track and vehicle-slab coupled system [12, 13]. Wang et al. established a spatial dynamic model of train steel-spring floating-slab-track interaction and analyzed the vibration characteristics of train passing through the steel-spring floating-slab track [14]. Huang et al. built a vehicle-track coupled dynamic system and investigated how the parameters of the floating-slab track and the train's speed influence the vehicle-track coupling system [15]. Liang et al. investigated the vibration characteristics of the damping-pad floating slab on the long-span steel-truss cable-stayed bridge in urban rail transit by developing a theoretical model of the train-track-bridge coupling interaction in the frequency domain [16]. Lu et al. established a vehicle-track dynamic interaction model to investigate the wheel-rail interaction characteristics of the steel-spring floating-slab track and carried out the dynamic analysis between the subway vehicle and the steel-spring floating-slab track under emergency braking conditions [17].

At the same time, in the research of the new floating-slab track structure that has side-mounted isolator to reduce lateral vibration, Park et al. proposed a new type of vibration isolator to overcome the shortcomings of the conventional floating-slab track and achieved good results [18]. Zhu et al. effectively suppressed the low-frequency vibration of the steel-spring floating-slab track by using a dynamic vibration absorber [19]. Ding et al. obtained the low-frequency vibration performance of the floating slab by vibration testing of the floating-slab track and optimized the parameters of the floating slab [20]. The above researches have achieved certain results in the optimization and improvement of the floating-slab structural parameters, but there is no research on the effect of lateral displacement limit effect of the floating slab.

The existing researches considered the interaction principles between the subway train and the steel-spring floating-slab track under normal circumstances and lower speed [21, 22]. Currently, there is still limited experience in applying steel-spring floating-slab track in urban express rail transit for higher speed worldwide. Therefore, this study focuses on the use of prefabricated steel-spring floating-slab track in urban express rail transit for higher speed. The wheel-rail dynamic performance under high-speed conditions was investigated by applying vehicle-track coupled dynamics theory and simulation technology. The analysis and evaluation of the vehicle-track dynamics, the vehicle operational safety, ride comfort, and track structural stability, were conducted according to Chinese railway dynamic performance evaluation standards. Ultimately, the study aimed to demonstrate the feasibility of using prefabricated steel-spring floating-slab track for urban express rail transit at very high running speed. In the developed model, optimization of the key structural parameters of the floating-slab track was performed to provide the theoretical basis and technical support for its engineering design and application to urban express rail transit.

2. Theoretical Model and Analysis of Vehicle-Track Coupled Dynamics

2.1. Vehicle-Track Coupled Dynamics Model of Steel-Spring Floating-Slab Track. The study proposes a model to simulate the dynamic interaction between the vehicle and the floating-slab track in order to effectively evaluate the running safety and stability of an intercity electric multiple-unit (EMU) train under conditions of different running speeds and floating-slab-track bearing stiffness. In addition, floating-slab-track vibration characteristics were investigated. The vehicle-track coupled dynamics model of the intercity EMU train was based on vehicle-track coupled-dynamics theory [23] (Figure 1). In the model, the vehicle is simulated as a rigid multicomponent system consisting of a car body, a frame, and a wheelset.

The lateral, vertical, side roll, shake, and nod movements of each part were considered. The rail is simulated as a Bernoulli-Euler beam supported on a base of elastic points. The rail-support points are arranged according to the actual fastener nodes' spacing by considering lateral, vertical, and rotational degrees of freedom. The vertical direction of the floating slab is simulated as a bidirectional curved elastic thin slab on an elastic foundation; the lateral direction is simulated as a rigid body, considering translational and rotational degrees of freedom. The concrete foundation is also simulated as a bidirectional curved elastic thin slab on the elastic foundation. The wheel-rail normal force was determined by the Hertz nonlinear elastic-contact theory, and the tangential force was determined by the nonlinear creep theory [24].

2.1.1. Vehicle Dynamic Equations. According to the multibody system dynamics, the vehicle subsystem is built by considering seven rigid parts involving a car body, two bogies, and four wheelsets with the primary and the secondary suspensions. Each component is, respectively, assigned with 5 degrees of freedom (DOFs) involving the vertical displacement Z, the lateral displacement Y, the roll angle Φ, the yaw angle Ψ, and the pitch angle β. Therefore, the vehicle subsystem has a total of 35 DOFs. For more details about the vehicle dynamic equations, monograph [25] can be consulted for readers.

2.1.2. Track Dynamic Equations. According to the method mentioned in [26], the track model consists of rail and floating slab. The vibrations of both were considered at the same time. The equations of motion are shown in (1)–(5).

(1) Rail dynamic equation

The rail is treated as a Bernoulli-Euler beam resting on the rail pads, and the lateral, vertical, and torsional vibrations are simultaneously taken into account. By adopting the modal superposition method, the second-order ordinary differential equations of the rail vibration can be obtained:

$$\ddot{q}_{zk}(t) + \frac{E_r I_y}{\rho_r A_r}\left(\frac{k\pi}{l}\right)^4 q_{zk}(t) = -\sum_{i=1}^{N_s} F_{rVi} Z_k(x_{Fi}) + \sum_{j=1}^{N_w} F_{Vi} Z_k(x_{Pi}), \quad k = 1 \sim N_Z, \tag{1}$$

$$\ddot{q}_{yk}(t) + \frac{E_r I_z}{\rho_r A_r}\left(\frac{k\pi}{l}\right)^4 q_{yk}(t) = -\sum_{i=1}^{N_s} F_{rHi} Z_k(x_{Fi}) + \sum_{j=1}^{N_w} P_{Hi} Z_k(x_{Pi}), \quad k = 1 \sim N_Y, \tag{2}$$

$$\ddot{q}_{tk}(t) + \frac{G_r J_z}{\rho_r J_r}\left(\frac{k\pi}{l}\right)^4 q_{tk}(t) = -\sum_{i=1}^{N_s} F_{rTi} \Phi_k(x_{Fi}) + \sum_{j=1}^{N_w} P_{Tj} \Phi_k(x_{Pi}), \quad k = 1 \sim N_T, \tag{3}$$

where E_r and G_r are Young's modulus and shear modulus of the rail, respectively; A_r and ρ_r are the cross-sectional area and mass density of the rail, respectively; J_{ry}, and J_{rz} are, respectively, the moments of inertia of the rail section to the lateral and vertical axes; J_{r0} and J_{rt} are the polar moments of inertia and torsional moment of inertia of the rail section, respectively; N_s and N_w are the numbers of sleepers and the number of axles in the rail section; F_{rVi}, F_{rHi}, and F_{rTi} are the vertical reaction force, lateral reaction force, and torsion reaction force of the i-th fulcrum of the rail, respectively; P_{Vj}, P_{Hj}, and P_{Tj} are the vertical force, lateral force, and torque of the rail acted by j-th wheel, respectively; and x_{Fj} and x_{Pj} are the x-coordinate of the i-th fulcrum of the rail and the x-coordinate of the j-th wheel set, respectively.

(2) Floating-slab dynamic equation

The floating slab is regarded as an elastic thin plate, whose governing equation is given by

$$\begin{aligned}&\frac{\partial^4 z_s(x,y,t)}{\partial x^4} + 2\frac{\partial^4 z_s(x,y,t)}{\partial x^2 \partial y^2} + \frac{\partial^4 z_s(x,y,t)}{\partial y^4} + \frac{C_s}{D_s}\\ &\quad + \frac{\partial z_s(x,y,t)}{\partial t} + \frac{\rho_s h_s}{D_s}\frac{\partial^4 w(x,y,t)}{\partial t^2}\\ &= \frac{1}{D_s}\left[\sum_{i=1}^{N_p} P_{rVi}(t)\delta(x - x_{Pi})\delta(y - y_{Pi})\right.\\ &\quad - \sum_{j=1}^{N_F} P_{sVj}(t)\delta\left(x - x_{Fj}\right)\delta\left(y - y_{Fj}\right)\\ &\quad \left. - \sum_{k=1}^{N_C} P_{cVk}(t)\delta(x - x_{Ck})\delta(y - y_{Ck})\right],\end{aligned} \tag{4}$$

where P_{rVi} is the vertical force of the i-th rail fastener point on the track slab; F_{sVj} is the vertical reaction force of the j-th steel spring isolator under the track slab; F_{cVk} is the vertical shear force of the k-th force hinge between the floating slabs; $z_s(x, y, t)$ is the vertical displacement or deflection of the floating slab; x_{Pi} and y_{Pi} are the positions of the i-th rail fasten points on the floating slab; x_{Fj} and y_{Fj} are the positions of the j-th steel spring isolators under the floating slab; x_{Ck} and y_{Ck} are the positions of the k-th shear joints between the floating slabs; and h_s, ρ_s, C_s, E_s, v_s, and D_s are slab thickness, density, damping coefficient, modulus of elasticity, Poisson's ratio, and bending stiffness, respectively.

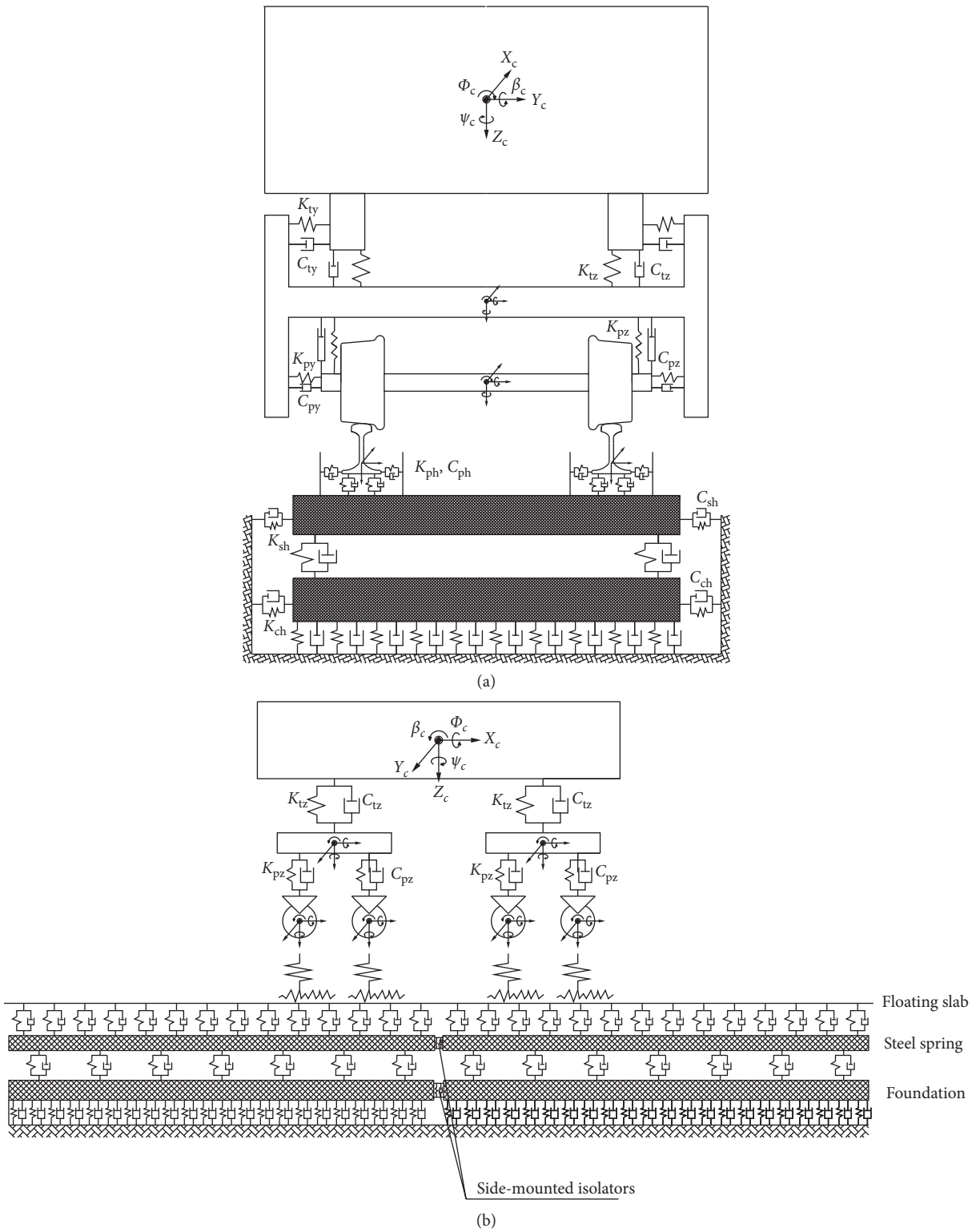

Figure 1: Vehicle-track coupled dynamics model of steel-spring floating-slab track. (a) End view. (b) Front view.

The generalized coordinate $T_{mn}(t)$ of the floating slab is introduced, and the above partial differential equation is converted into a second-order ordinary differential equation by the Ritz method, as shown in equation (7):

$$\ddot{T}_{mn}(t) + \frac{C_s}{\rho_s h_s}\dot{T}_{mn}(t) + \frac{D_s}{\rho_s h_s}\frac{B_3B_2 + 2B_4B_5 + B_1B_6}{B_1B_2}T_{mn}(t)$$
$$= \frac{1}{\rho_s h_s B_1 B_2}\left[\sum_{i=1}^{N_P} P_{rVi}(t)X_m(x_{Pi})Y_n(y_{pi}) - \sum_{j=1}^{N_F} F_{sVj}(t)\right.$$
$$\left.\cdot X_m(x_{Fj})Y_n(y_{Fj}) - \sum_{k=1}^{N_C} F_{cVk}(t)X_m(x_{Cj})Y_n(y_{Cj})\right], \tag{5}$$

where $m = 1, 2, \ldots, N_x$ and $n = 1, 2, \ldots, N_y$.

$$\begin{cases} B_1 = \int_0^{L_s} X_m^2(x)\mathrm{d}x, \\ B_2 = \int_0^{W_s} Y_n^2(y)\mathrm{d}y, \\ B_3 = \int_0^{L_s} X'''_m(x)X_m(x)\mathrm{d}x, \\ B_4 = \int_0^{L_s} X''_m(x)X_m(x)\mathrm{d}x, \\ B_4 = \int_0^{W_s} Y''_n(y)Y_n(y)\mathrm{d}x, \\ B_4 = \int_0^{W_s} Y'''_n(y)Y_n(y)\mathrm{d}x. \end{cases} \tag{6}$$

At moment t, the vertical displacement at point (x, y) of the track is

$$z_s(x, y, t) = \sum_{m=1}^{N_x}\sum_{n=1}^{N_x} X_m(x)Y_n(y)T_{mn}(t), \tag{7}$$

where N_x and N_y are the cutoff mode orders of directions for length and width of the floating slab, respectively, and $X_m(x)$ and $Y_n(y)$ are the beam-mode functions of directions for length and width of the floating slab, respectively.

2.2. The Wheel and Rail Interaction Principle. The vehicle-floating-slab track (FST) is a dynamic interaction system, and the wheel-rail relationship is the link between the vehicle subsystem and the track subsystem. In previous vehicle-track dynamics equations, if the wheel-rail interaction force was determined, the numerical simulation method was applied, and the dynamics simulation analysis of the vehicle-track system could be performed. In this research, the wheel-rail contact geometry was determined according to the principle of wheel-rail contact mentioned in [27]. The wheel and rail normal force and wheel and rail creep force were calculated according to the method mentioned in [26, 28]. On obtaining the wheel-rail force, the values can be substituted into the dynamic equations of the vehicle and the track as the reaction force of the wheel and the external load of the track.

2.3. Track Irregularities. Because the vehicle-track coupled dynamic system is very complicated and extensive, a fast explicit-integration method should be used to solve its dynamic response problem [29]. At present, China has no reliable track-irregularity data for urban express rail transit. For the purpose of analysis, considering the characteristics of the floating-slab track and the deterioration of railway-line smoothness after long-term operation, the excitation input of the vehicle-track dynamic system was based on the U.S. six-grade track spectrum that closely matches the Chinese urban express rail transit [30]. Accordingly, the power-spectral-density expressions of the track-vertical-profile, track-alignment, rail-gauge, and track-cross-level irregularities can be expressed as shown in equations (10) and (11):

(1) Track-vertical-profile irregularity:

$$S_v(\Omega) = \frac{kA_v\Omega_c^2}{\Omega^2\left(\Omega^2 + \Omega_c^2\right)}, \tag{8}$$

where $S_v(\Omega)$ is the power-spectral density of track-vertical-profile irregularity [cm^2/(rad/m)], A_v is the roughness constant (cm^2·rad/m), Ω_c is the cutoff frequency (rad/m), and k is the safety coefficient.

(2) Track-alignment irregularity:

$$S_a(\Omega) = \frac{kA_v\Omega_c^2}{\Omega^2\left(\Omega^2 + \Omega_c^2\right)}, \tag{9}$$

where $S_v(\Omega)$ is the power-spectral density of track-alignment irregularity [cm^2/(rad/m)], A_a is the roughness constant (cm^2·rad/m), and Ω_c is the cutoff frequency (rad/m).

(3) Rail-gauge and track-cross-level irregularities:

$$S_c(\Omega) = S_g(\Omega) = \frac{4kA_v\Omega_c^2}{\left(\Omega^2 + \Omega_s^2\right)\left(\Omega^2 + \Omega_c^2\right)}, \tag{10}$$

where $S_c(\Omega)$ and $S_g(\Omega)$ are the power-spectral densities of rail-gauge and track-cross-level irregularities [cm^2/(rad/m)], respectively, and Ω_s is the cutoff frequency (rad/m).

According to the track power spectrum density expression, a new algorithm based on the frequency domain power spectrum equivalent was used to obtain the amplitude and stochastic phase of the spectrum. The inverse Fourier transform was used to obtain time-domain samples of the stochastic irregularity of the track (Figures 2~5), which were used as the excitation input of the vehicle-track dynamics system.

2.4. Numerical Integration Method. It can be seen that the developed dynamics model has large DOFs involving many nonlinear factors and time-varying parameters. Consequently, an efficient numerical integration algorithm is essential for this problem. In this paper, the Zhai method [31]

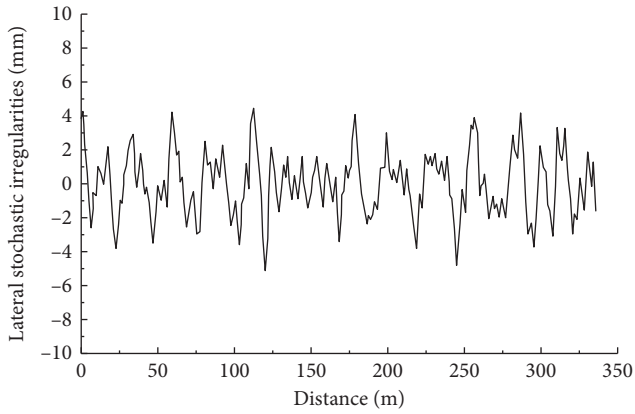

Figure 2: Lateral stochastic irregularities in the left rail.

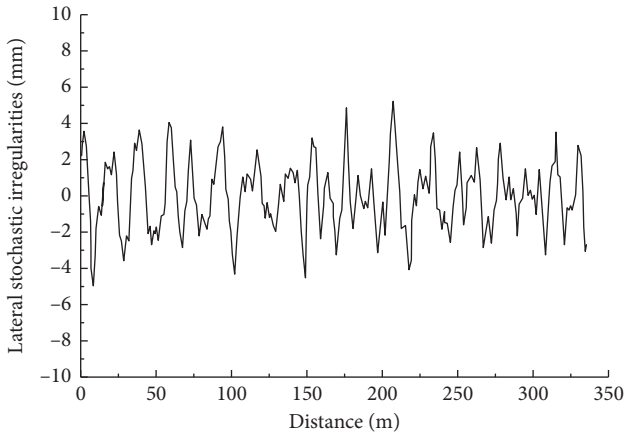

Figure 3: Lateral stochastic irregularities in the right rail.

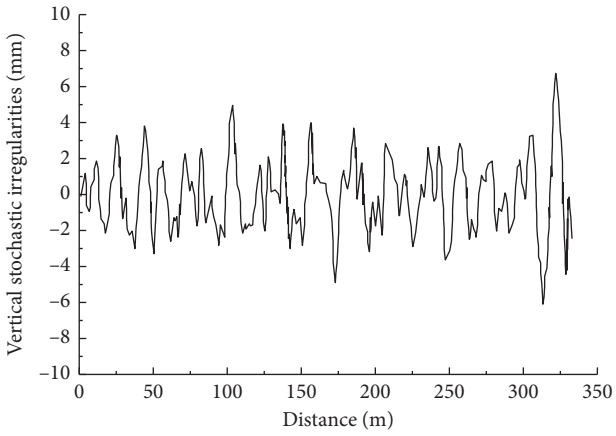

Figure 4: Vertical stochastic irregularities in the left rail.

is adopted to solve such a large-scale dynamic model, which has the integration form as follows:

$$\begin{cases} X_{n+1} = X_n + \dot{X}_n \Delta t + (0.5 + \psi)\ddot{X}_n \Delta t^2 - \psi \ddot{X}_{n-1} \Delta t^2, \\ \dot{X}_{n+1} = \dot{X}_n + (1 + \varphi)\ddot{X}_n \Delta t - \varphi \ddot{X}_{n-1} \Delta t, \end{cases} \tag{11}$$

where X, $\dot{X}$, and $\ddot{X}$ are the generalized displacement, velocity, and acceleration of the system, respectively; Δt is the time step for numerical integration; the independent parameters φ and ψ are used for controlling the stability of the algorithm; the subscript n indicates the integration at the time of $n\Delta t$.

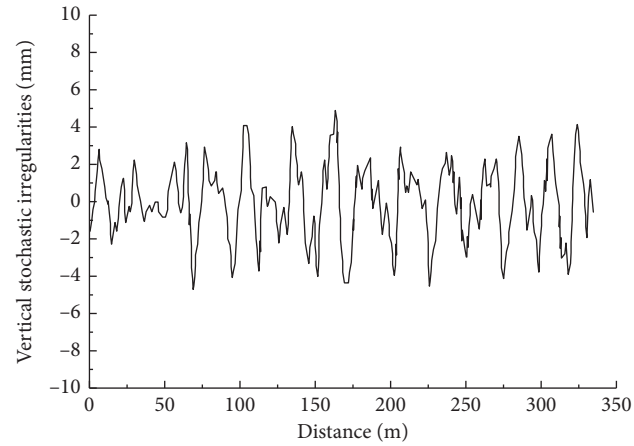

Figure 5: Vertical stochastic irregularities in the right rail.

3. Basic Parameters for Dynamic Analysis

3.1. Vehicle Parameters. The fully loaded CRH6 intercity EMU train was considered as model vehicle when setting the vehicle parameters required for the vehicle-track-coupled dynamics simulation while keeping the overall parameters within safety limits (Table 1).

3.2. Rail Parameters. To ensure overall vehicle safety, the full-load parameters for the CRH6 intercity EMU train were considered. The basic calculation parameters for the rail are shown in Table 2.

3.3. Floating-Slab-Track Parameters and Layout Scheme. We studied and analyzed mainly 3.6 m and 4.8 m long floating-slab tracks. In order to reduce the vertical displacement at the joint of adjacent floating slabs, an increase in the stiffness transition of the floating slab by side-mounted vibration isolator was proposed. The side-mounted isolator was added to each end of the floating slab, as shown in Figures 6~8.

The basic parameters of the 3.6 m long prefabricated floating slab are shown in Table 3, and layout schematics are shown in Figures 9–11.

The basic parameters of the prefabricated 4.8 m long floating slab are shown in Table 4, and layout schematics are shown in Figures 6, 12, and 13.

3.4. Model Reliability Verification. Here only the verification results of the vibration response of the floating slab are provided. Figure 7 shows comparison of the results and analysis of the vertical vibration acceleration of the floating-slab track bed in a straight section of a subway line, with train passing speed about 55 km/h. According to the vibration response results at a cross section of the floating-slab bed

Table 1: Basic parameters of CRH6 intercity EMU train.

Parameter name	Value	Unit
Vehicle parameters		
Bogie center distance (vehicle distance)	17,500	mm
Wheelbase	2500	mm
Wheel rolling-circle lateral span	1493	mm
Wheel rolling-circle diameter	860	mm
Wheelset inner distance	1353	mm
Wheel shape	LMA	—
Rail shape	CHN60	—
Mass/moment of inertia and center of gravity		
Car-body quality	37.2	t
Body-roll moment of inertia	107.6	$t \cdot m^2$
Car-body nodding moment of inertia	1426.8	$t \cdot m^2$
Car-body shaking head moment of inertia	1402.7	$t \cdot m^2$
Car-weight heart distance from rail surface	1.712	m
Frame quality	2.70	t
Frame roll moment of inertia	2.19	$t \cdot m^2$
Frame nodding moment of inertia	1.48	$t \cdot m^2$
Frame moving-head moment of inertia	2.70	$t \cdot m^2$
Height of gravity center of frame	0.5	m
Wheelset quality	1.935	t
Wheelset rolling moment of inertia	0.95	$t \cdot m^2$
Wheelset nodding moment of inertia	0.15	$t \cdot m^2$
Wheelset shaking moment of inertia	0.95	$t \cdot m^2$
Structural parameters		
Primary suspension		
Half distance of lateral span	2.10	m
Height of upper spring-loaded point from rail surface	0.876	m
Height of lower spring-loaded point from rail surface	0.681	m
Half distance of vertical-damping lateral span	2.10	m
Longitudinal damping from vertical distance to center of bogie	1.491	m
Height of upper vertical-damping point from rail surface	0.9	m
Height of lower vertical-damping point from rail surface	0.48	m
Half distance of lateral span of axle-box boom node	2.10	m
Height of axle-box boom node from rail surface	0.46	m
Longitudinal distance of axle-box arm node from center of bogie	0.77	m
Secondary suspension		
Air-spring lateral span	2.02	m
Height of upper surface of air spring from rail surface	0.884	m
Height of lower surface of air spring from rail surface	0.633	m
Lateral span of anti-movement-of-snake damper	2.6	m
Longitudinal distance between anti-movement-of-snake damper and body-connection point from center of car body (inside center pin)	9.51	m
Longitudinal distance between anti-movement-of-snake damper and frame-connection point from center of car body (inside center pin)	8.79	m
Height of anti-movement-of-snake damper and car-body-connection point from rail surface	0.556	m
Height of anti-movement-of-snake damper and frame-connection point from rail surface	0.492	m
Longitudinal distance of lateral damper from center of car body	8.9	m
Lateral distance between lateral damper and vehicle-body-connection point from center line of vehicle body	1.4	m
Lateral distance between lateral damper and frame-connection point from center line of vehicle body	0.933	m
Height of lateral damper and body-connection point from rail surface	0.764	m
Height of lateral damper and frame-connection point from rail surface	0.724	m
Vertical distance of vertical damper from center of car body	8.2	m
Lateral distance between vertical damper and vehicle-body-connection point from center line of vehicle body	1.323	m
Lateral distance between vertical damper and frame-connection point from center line of vehicle body	1.323	m
Height of vertical damper and body-connection point from rail surface	0.81	m
Height of vertical damper and frame-connection point from rail surface	0.382	m
Lateral-stop lateral span	0.211	m
Height of lateral stop from rail surface	0.49	m
Height of anti-rolling torsion bar from rail surface	0.792	m

Table 1: Continued.

Parameter name	Value	Unit
Anti-rolling torsion-bar-mount lateral span	0.952	m
Longitudinal distance of anti-rolling torsion bar from center of bogie	0.4	m
Height of connection point between traction pin and vehicle body from rail surface	0.884	m
Suspension parameters		
Primary suspension		
Steel-spring longitudinal stiffness (per axle box) (including damping pad)	0.9	MN/m
Steel-spring lateral stiffness (per axle box) (including damping pad)	0.9	MN/m
Steel-spring vertical stiffness (per axle box)	1.30	MN/m
Vertical damping (per axle box)	9.8	kN·s/m
Vertical-damper series stiffness	3.5	MN/m
Axle-box boom-joint longitudinal stiffness (per axle box)	17.1	MN/m
Axle-box boom-joint lateral stiffness (per axle box)	6.1	MN/m
Secondary suspension		
Air-spring longitudinal/lateral stiffness	0.20	MN/m
Air-spring vertical stiffness	0.22	MN/m
Air-spring emergency rubber stiffness	13.7	MN/m
Stiffness between emergency spring and upper cover	36	mm
Lateral-damper series stiffness	3.75	MN/m
Anti-movement-of-snake-damper series stiffness	8	MN/m
Vertical damping	9.8	kN·s/m
Lateral-stop free clearance	20	mm
Anti-rolling torsion-bar equivalent stiffness (single bogie)	3.0	MNm/rad

Table 2: Basic parameters of rail.

Parameter name	Value	Unit
Rail elastic modulus	2.059×10^{11}	Pa
Rail Poisson's ratio	0.3	—
Rail density	7.83×10^{3}	kg/m^3
Rail shape	CN60	—
Fastener vertical stiffness	3.0×10^{7}	N/m
Fastener lateral stiffness	2.0×10^{7}	N/m
Fastener vertical damping	7.5×10^{4}	N·s/m
Fastener lateral damping	5.0×10^{4}	N·s/m
Fastener spacing	0.600/0.625	m

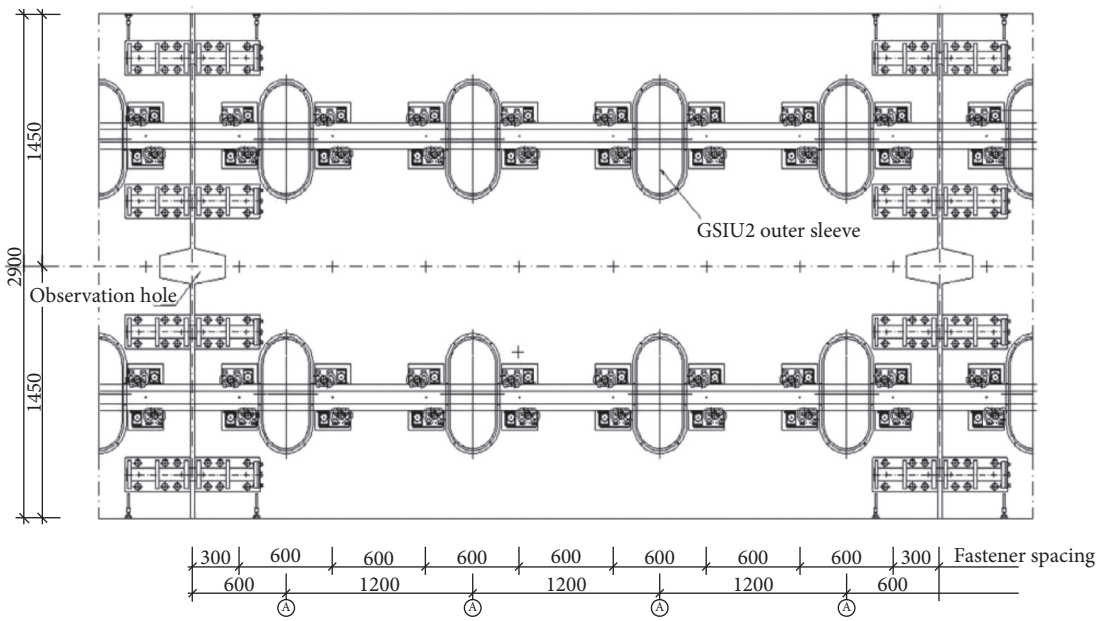

Figure 6: Plan view of the prefabricated 4.8 m long floating-slab transition board.

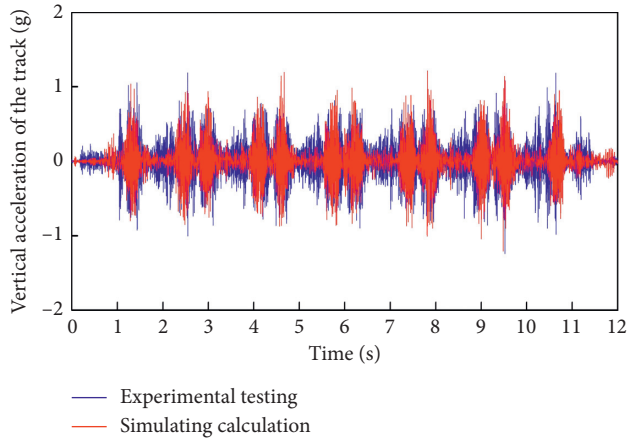

Figure 7: Comparison of vibration acceleration of floating slab obtained by test and simulation.

Figure 8: Steel-spring floating-slab-track isolator.

Table 3: Basic parameters of the 3.6 m long prefabricated floating slab.

Parameter name	Value
Vibration-isolator model	GSIU (double cylinder) isolator
Vibration-isolator stiffness	Vertical stiffness: 13.2 kN/mm Lateral stiffness: 9.8 kN/mm
Vibration-isolator damping	Vertical damping: 0–100 N·s/mm Lateral damping: 40.0 N·s/mm
Inside-isolator spacing	1800 mm
Floating-slab length	3600 mm
Floating-slab width	2900 mm
Floating-slab thicknesses	350 mm, 450 mm, 550 mm
Floating-slab and other track-bed stiffness transition modes	1 to 5 transition slabs are placed adjacent to other track beds (inside isolators are spaced 1200 mm apart)

(Figure 7), it can be easily distinguished that the vibration acceleration responses were pronounced at measurement points when the subway vehicle is passing through. When the bogies of subway vehicle pass through the vibration measuring points, the vibration accelerations of the floating slab bed have obvious fluctuations. In the simulation calculation, the vertical acceleration of the floating-slab track bed can more clearly reflect the vibration state of each wheel set when the vehicle is passing through the measurement points.

The vertical vibration acceleration test and simulation calculations of the floating-slab track bed have maximum values of 1.22 g and 1.18 g and effective values of 0.172 g and 0.163 g, respectively. The simulation calculation results are slightly smaller than the test results, but they are all within the acceptable error range. The above results show that the simulation calculation model can better reflect the vibration response process of the floating slab bed. The intercity train vehicle-floating-slab track dynamic model established in this paper can be used to evaluate the wheel-rail dynamic performance of floating-slab bed under fast driving conditions.

4. Analysis of Driving Safety and Stability Running on Prefabricated Steel-Spring Floating Slab

4.1. Analysis of the Influence of the Length of the Floating Slab on Vehicle-Track Dynamics Characteristics. On the basis of the Chinese railway code [32, 33], the 3.6 m and 4.8 m long prefabricated steel-spring floating-slab tracks were chosen as focus of this research. The safety, stability, and comfort of CRH6 intercity EMU trains running at different speeds and on different radial lines were

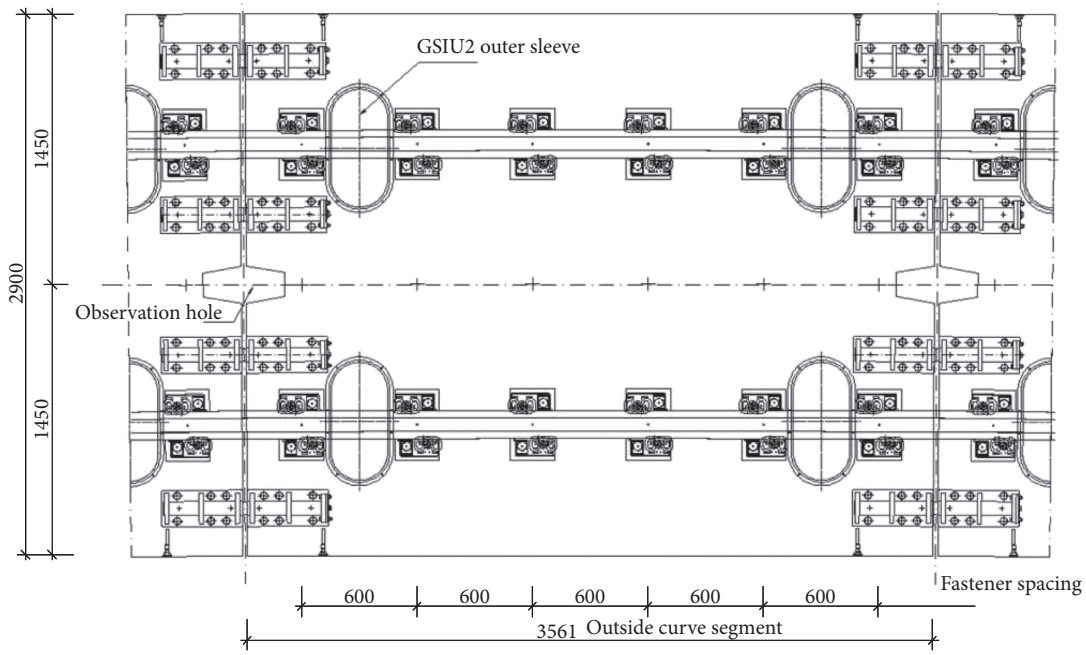

Figure 9: Prefabricated 3.6 m long floating-slab track.

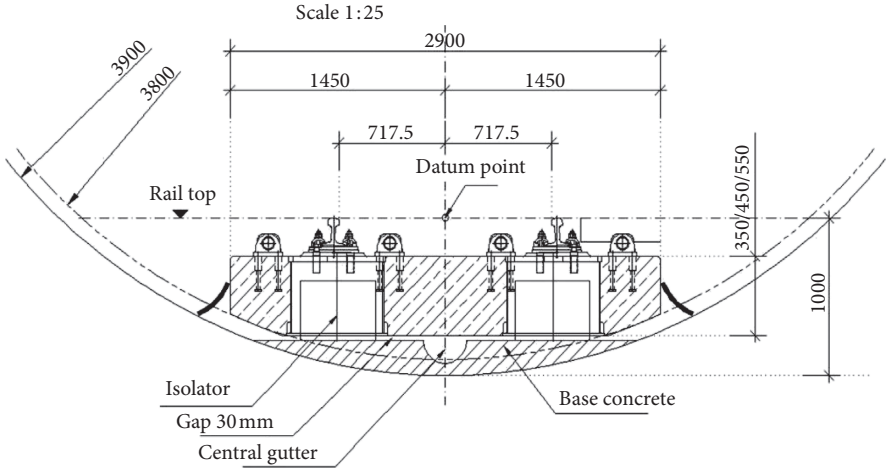

Figure 10: Sectional view of the prefabricated 3.6 m long floating-slab track.

investigated. Also, the performance and the stability of the track itself were analyzed. The working conditions (Tables 5–13) considered in this study are straight line-140, straight line-160, and straight line-200, which indicates that the intercity EMU train passes through a straight line at the speeds of 140, 160, and 200 km/h, respectively, and Curve-140 and Curve-160, which indicates that the intercity EMU train travels the curve sections of $R = 1100$ m and $R = 1500$ m at the speeds of 140 and 160 km/h, respectively. L values of 3.6 and 4.8 m indicate the two lengths of the prefabricated steel-spring floating-slab track. The calculation results of wheel-rail-system dynamic response, vehicle stability and comfort, rail dynamic response, and floating-slab dynamic response under various conditions are shown in Tables 5–8. These tabulated results suggest the following:

(i) When the intercity EMU train runs on either the 3.6 m or 4.8 m long prefabricated floating track beds, its dynamic performance is basically the same, although the stability of the 3.6 m floating slab is slightly lower than that of the 4.8 m slab.

(ii) Whether the intercity EMU train runs at 140, 160, or 200 km/h on the straight sections and 140 or 160 km/h in the curved sections ($R = 1100$ m or $R = 1500$ m) of either the 3.6 m or 4.8 m prefabricated floating-slab-track bed, the wheel-axle lateral force, the wheel-rail vertical force, the derailment coefficient, and the wheel-load shedding rate are all less than the specified code limit. The lateral acceleration of the body is lower than the specified code limit, the stability index is "excellent," and the comfort rating is "comfortable."

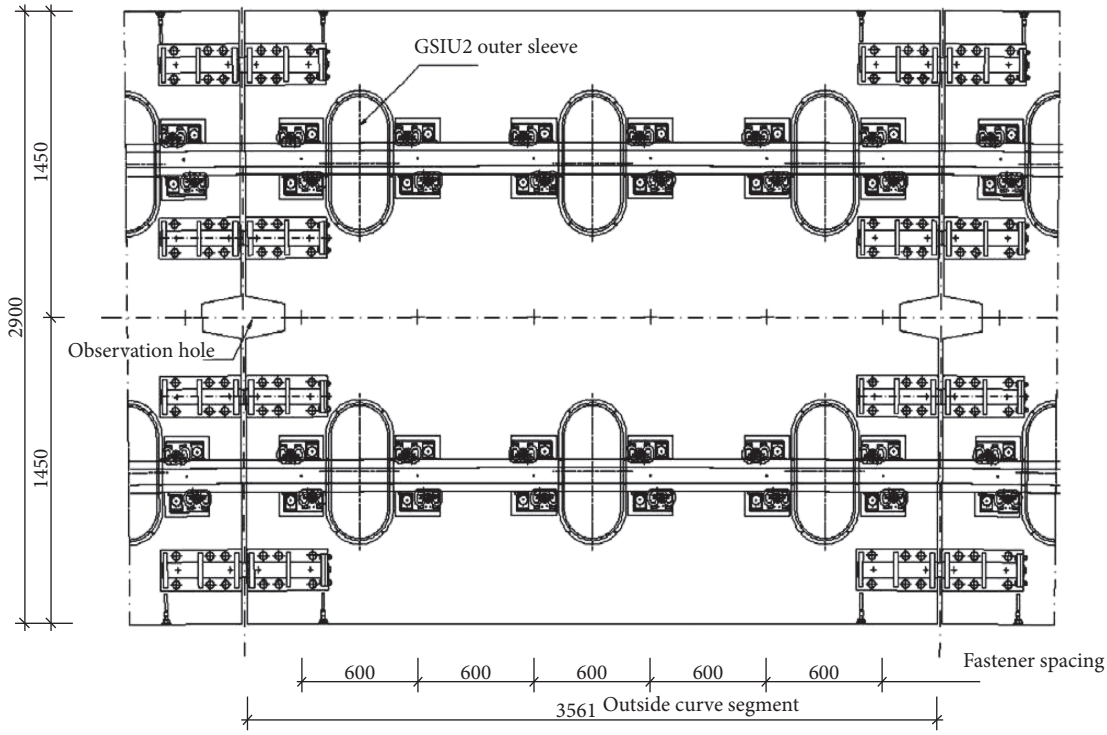

Figure 11: Plan view of the prefabricated 3.6 m long floating-slab-track transition-slab.

Table 4: Basic parameters of the prefabricated 4.8 m long floating-slab track.

Parameter name	Value
Vibration-isolator model	GSIU (double cylinder) isolator
Vibration-isolator stiffness	Vertical stiffness: 13.2 kN/mm Lateral stiffness: 9.8 kN/mm
Vibration-isolator damping	Vertical damping: 0–100 N·s/mm Lateral damping: 40.0 N·s/mm
Inside-isolator spacing	1800 mm
Length of floating slab	4800 mm
Width of floating slab	2900 mm
Thickness of floating slabs	350 mm, 450 mm, 550 mm
Floating-slab and other track-bed stiffness transition modes	1 to 5 transition slabs are placed adjacent to other track beds (in-slab isolators are spaced 1200 mm apart)

4.2. Analysis of the Influence of the Track-Slab Thickness on Vehicle-Track Dynamics Characteristics. To investigate the influence of floating-slab thickness on the vehicle-track dynamics characteristics, analysis of the stability and safety of the vehicles using three different thicknesses for the steel-spring floating-slab-track beds, namely, 350, 450, and 550 mm (Tables 9–13), was performed. Assuming that other parameters are unchanged, the vertical displacement of the rail, vertical-vibration acceleration of the rail, vertical displacement at the center part of the floating slab, radial acceleration of the vertical vibration of the floating slab, lateral displacement of the floating slab, root mean square of the lateral-vibration acceleration of the floating slab, derailment coefficient, wheel-load shedding rate, lateral stability of the vehicle body, and ride-comfort indicator of the floating slab were calculated. The results are shown in Tables 9–13.

Calculations regarding thickness and dynamics characteristics suggest the following:

(i) In general, the influence of thickness variation of the 3.6 m and 4.8 m long prefabricated steel-spring floating-slab-track beds on the vertical displacement of rail, vertical-vibration acceleration of rail, vertical displacement of the central part of the floating slab, and the vertical-vibration acceleration of the floating slab is not apparent.

(ii) With the increase in thickness of the 3.6 m and 4.8 m long prefabricated steel-spring floating-slab-track beds, the vertical displacement of the rail slightly increased, lateral displacement and acceleration of the rail decreased to a great extent, and the lateral displacement and lateral acceleration of the rail slab decreased. In addition, as the slab

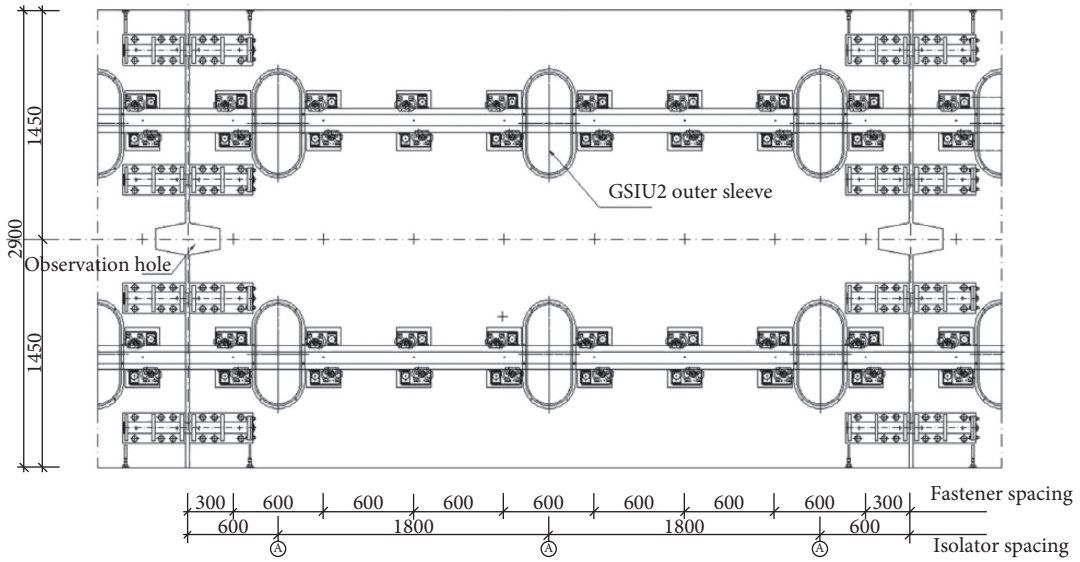

Figure 12: Plan view of the prefabricated 4.8 m long floating slab.

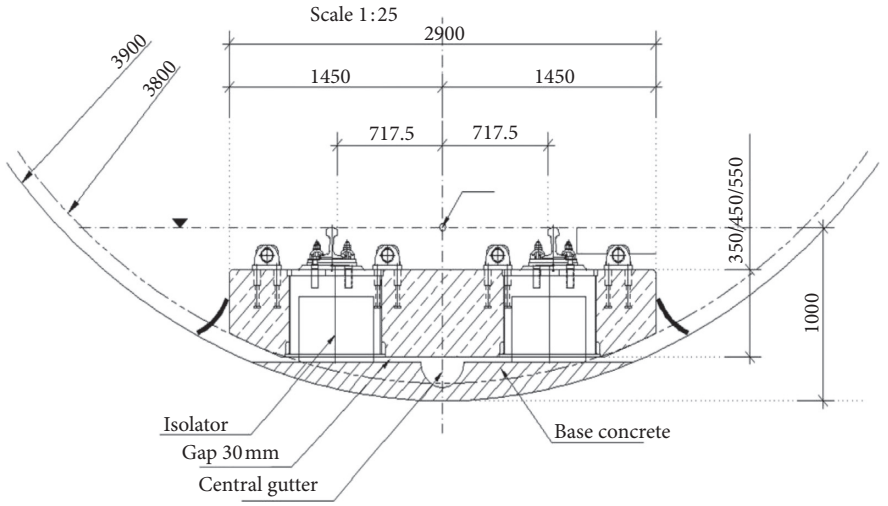

Figure 13: Sectional view of the prefabricated 4.8 m long floating slab.

Table 5: Wheel-rail safety indicators for floating-slab-track bed.

Calculation working condition	Wheel-axle lateral force (kN)		Wheel-rail vertical force (kN)		Derailment coefficient		Wheel-load shedding rate	
	$L = 3.6$ m	$L = 4.8$ m	$L = 3.6$ m	$L = 4.8$ m	$L = 3.6$ m	$L = 4.8$ m	$L = 3.6$ m	$L = 4.8$ m
Straight line-140	12.331	12.188	76.143	77.956	0.184	0.186	0.155	0.158
Straight line-160	12.913	12.890	79.518	80.343	0.182	0.187	0.187	0.179
Straight line-200	14.979	13.598	88.942	90.019	0.198	0.196	0.281	0.269
Curve-140	29.434	29.592	86.295	89.322	0.309	0.315	0.302	0.294
Curve-160	28.538	28.423	86.950	87.968	0.290	0.291	0.336	0.310
Specified code limits [32, 33]	60.92		250		1.0		0.90	

L: length.

Table 6: Vehicle-stability and comfort indicators for floating-slab-track bed.

Calculation working condition	Vehicle-body lateral acceleration (g)		Vehicle-body vertical acceleration (g)		Lateral-stability index		Vertical-stability index		Comfort index	
	$L = 3.6$ m	$L = 4.8$ m	$L = 3.6$ m	$L = 4.8$ m	$L = 3.6$ m	$L = 4.8$ m	$L = 3.6$ m	$L = 4.8$ m	$L = 3.6$ m	$L = 4.8$ m
Straight line-140	0.032	0.034	0.047	0.042	1.707	1.708	1.549	1.558	0.733	0.733
Straight line-160	0.033	0.036	0.053	0.048	1.945	1.947	1.823	1.826	0.741	0.743
Straight line-200	0.040	0.040	0.057	0.053	2.002	2.005	1.870	1.871	0.914	0.919
Curve-140	0.058	0.057	0.045	0.041	2.117	2.115	1.619	1.626	1.102	1.105
Curve-160	0.067	0.065	0.049	0.045	2.185	2.181	1.649	1.652	1.199	1.196
Specified code limits [32, 33]	0.10		0.15		2.5 (excellent)		2.5 (excellent)		2.0 (comfortable)	

L: length.

Table 7: Vibration indicators of rail on floating-slab-track bed.

Calculation working condition	Rail vertical displacement (mm)		Rail vertical acceleration RMS value (g)		Rail lateral displacement (mm)		Rail lateral acceleration RMS value (g)	
	$L = 3.6$ m	$L = 4.8$ m	$L = 3.6$ m	$L = 4.8$ m	$L = 3.6$ m	$L = 4.8$ m	$L = 3.6$ m	$L = 4.8$ m
Straight line-140	2.546	2.454	5.897	5.753	0.209	0.253	0.286	0.275
Straight line-160	2.582	2.471	6.575	6.477	0.218	0.263	0.385	0.375
Straight line-200	2.683	2.540	7.613	7.408	0.375	0.356	0.635	0.639
Curve-140	2.670	2.603	5.671	5.606	0.292	0.320	0.997	1.003
Curve-160	2.698	2.601	6.483	6.329	0.286	0.303	1.068	1.077

RMS: root mean square; L: length.

Table 8: Vibration indicators of floating-slab track.

Calculation working condition	Track vertical displacement (mm)		Track vertical acceleration RMS value (g)		Track lateral displacement (mm)		Track lateral acceleration RMS value (g)	
	$L = 3.6$ m	$L = 4.8$ m	$L = 3.6$ m	$L = 4.8$ m	$L = 3.6$ m	$L = 4.8$ m	$L = 3.6$ m	$L = 4.8$ m
Straight line-140	2.016	1.849	0.611	0.624	0.104	0.118	0.024	0.036
Straight line-160	2.033	1.850	0.644	0.782	0.111	0.125	0.025	0.038
Straight line-200	2.039	1.859	0.730	0.912	0.244	0.217	0.040	0.042
Curve-140	1.990	1.772	0.646	0.770	0.145	0.195	0.048	0.050
Curve-160	1.999	1.789	0.713	0.967	0.103	0.170	0.049	0.054

RMS: root mean square; L: length.

Table 9: Vertical-vibration index of the rail.

Calculation working condition	Vertical displacement of the rail						RMS of lateral-vibration acceleration of the floating slab					
	$L = 3.6$ m			$L = 4.8$ m			$L = 3.6$ m			$L = 4.8$ m		
	350*	450*	550*	350*	450*	550*	350*	450*	550*	350*	450*	550*
Straight line-140	4.794	4.860	4.919	4.045	3.980	4.025	7.754	7.701	7.682	7.572	7.577	7.671
Straight line-160	4.891	4.983	5.058	4.038	4.124	4.240	8.669	8.566	8.579	8.482	8.472	8.443
Straight line-200	5.182	5.342	5.506	4.376	4.526	4.618	10.331	10.309	10.300	9.921	9.986	9.989
Curve-140	5.258	5.256	5.291	4.299	4.236	4.218	7.657	7.610	7.586	7.578	7.579	7.607
Curve-160	5.301	5.333	5.410	4.199	4.274	4.408	9.909	8.763	8.599	8.566	8.586	8.566
Maximum per 100 mm range of change (%)	3.1			3.4			11.6			1.2		

*Thickness (mm) of steel-spring floating-slab-track bed; L: length; RMS: root mean square.

Table 10: Vertical-vibration index of the floating slab.

Calculation working condition	Vertical displacement at the central part of the floating slab						RMS of vertical vibration acceleration in the middle of the floating slab					
	$L = 3.6$ m			$L = 4.8$ m			$L = 3.6$ m			$L = 4.8$ m		
	350	450	550	350	450	550	350	450	550	350	450	550
Straight line-140	3.863	3.797	3.757	3.095	3.090	3.233	1.032	1.334	0.914	0.968	0.953	1.073
Straight line-160	3.832	3.765	3.760	3.192	3.217	3.189	1.311	1.139	1.551	1.147	1.249	1.084
Straight line-200	3.797	3.881	3.861	3.121	3.127	3.123	1.366	1.556	1.318	1.238	1.513	1.235
Curve-140	3.732	3.675	3.714	3.321	3.051	3.459	1.219	1.390	1.319	1.125	1.226	1.513
Curve-160	3.750	3.734	3.752	3.368	3.215	3.383	1.146	1.444	1.164	1.284	1.494	1.171
Maximum per 100 mm range of change (%)		2.2			13.4			36.2			23.3	

L: length; RMS: root mean square.

Table 11: Lateral-vibration index of the floating slab.

Calculation working condition	Lateral displacement of the floating slab						RMS of lateral-vibration acceleration of the floating slab					
	$L = 3.6$ m			$L = 4.8$ m			$L = 3.6$ m			$L = 4.8$ m		
	350	450	550	350	450	550	350	450	550	350	450	550
Straight line-140	0.290	0.296	0.293	0.155	0.132	0.150	0.050	0.048	0.038	0.046	0.043	0.025
Straight line-160	0.339	0.374	0.383	0.155	0.201	0.224	0.058	0.051	0.053	0.040	0.043	0.030
Straight line-200	0.508	0.510	0.489	0.342	0.371	0.390	0.090	0.079	0.062	0.062	0.073	0.055
Curve-140	0.275	0.203	0.251	0.194	0.187	0.217	0.087	0.074	0.061	0.072	0.062	0.060
Curve-160	0.233	0.241	0.292	0.165	0.246	0.262	0.123	0.078	0.059	0.074	0.093	0.084
Maximum per 100 mm range of change (%)		26.2			49.3			37.0			42.3	

L: length; RMS: root mean square.

Table 12: Wheel-rail safety indicators of the floating-slab-track bed.

Calculation working condition	Derailment coefficient						Wheel-load shedding rate					
	$L = 3.6$ m			$L = 4.8$ m			$L = 3.6$ m			$L = 4.8$ m		
	350	450	550	350	450	550	350	450	550	350	450	550
Straight line-140	0.181	0.184	0.184	0.190	0.189	0.189	0.154	0.157	0.158	0.152	0.153	0.155
Straight line-160	0.181	0.182	0.180	0.190	0.188	0.186	0.178	0.180	0.183	0.175	0.179	0.180
Straight line-200	0.186	0.189	0.195	0.182	0.189	0.194	0.267	0.284	0.280	0.283	0.284	0.278
Curve-140	0.301	0.306	0.305	0.293	0.307	0.312	0.283	0.287	0.287	0.289	0.294	0.294
Curve-160	0.271	0.272	0.278	0.268	0.272	0.273	0.283	0.286	0.295	0.302	0.305	0.306
Specified code limit [32, 33]		2.5			4.8			6.2			2.1	

L: length.

Table 13: Vehicle-track stationary stability and comfort indicators of the floating-slab track.

Calculation working condition	Lateral-stability index						Comfort index					
	$L = 3.6$ m			$L = 4.8$ m			$L = 3.6$ m			$L = 4.8$ m		
	350	450	550	350	450	550	350	450	550	350	450	550
Straight line-140	1.701	1.700	1.698	1.708	1.708	1.709	0.737	0.736	0.734	0.741	0.746	0.749
Straight line-160	1.941	1.939	1.934	1.948	1.949	1.947	0.745	0.746	0.742	0.753	0.761	0.762
Straight line-200	2.003	2.006	2.002	2.007	2.005	2.002	0.930	0.942	0.942	0.931	0.936	0.936
Curve-140	2.120	2.117	2.112	2.122	2.121	2.120	1.105	1.099	1.092	1.119	1.119	1.119
Curve-160	2.179	2.173	2.174	2.181	2.179	2.176	1.207	1.197	1.187	1.200	1.202	1.198
Maximum per 100 mm range of change (%)		3.0			2.0			1.3			1.1	

L: length.

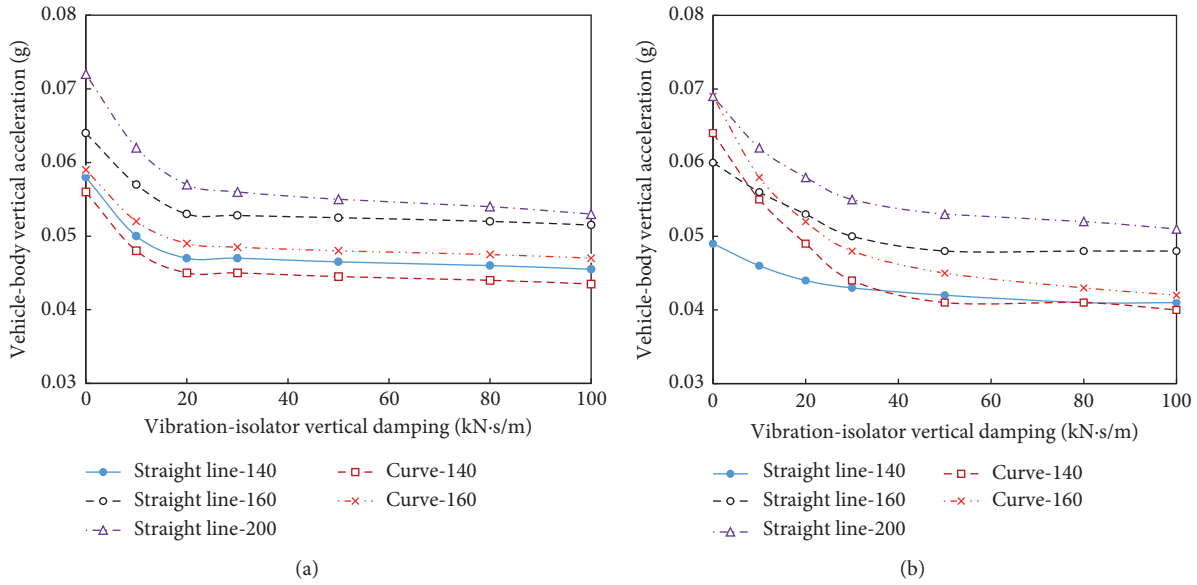

Figure 14: Variation of the vertical acceleration of the train with vibration isolator damping. (a) 3.6 m floating-slab track. (b) 4.8 m floating-slab track.

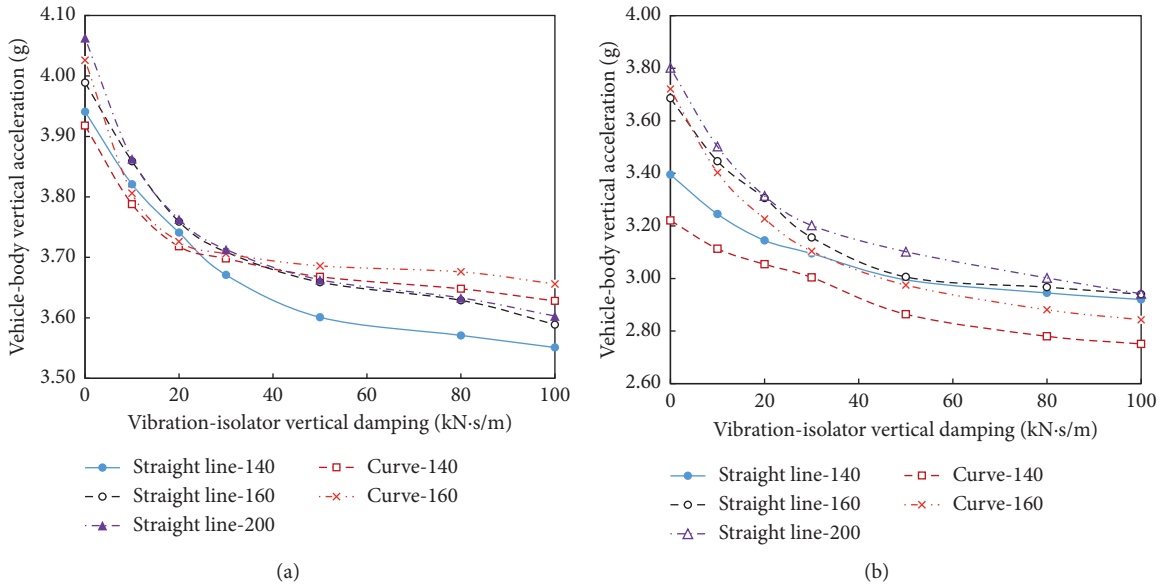

Figure 15: Variation of the vertical displacement of the train vibration isolator damping. (a) 3.6 m floating-slab track. (b) 4.8 m floating-slab track.

thickness increases, the vertical displacement of the track bed increases, and lateral stability improves.

(iii) The thickness variation of the 3.6 m and 4.8 m long prefabricated steel-spring floating-slab tracks has little effect on the operational-safety and ride-comfort indexes of the intercity EMU trains.

(iv) With the increase of the thickness of the 3.6 m and 4.8 m long prefabricated steel-spring floating-slab-track beds, the wheel and rail safety index slightly increased, and the vehicle-stability and ride-comfort indicators were slightly reduced. The reason for the increase in the wheel-rail safety index is that the increase in the thickness of the floating slab increases the wheel-rail impact at the transition joint of the track slab.

4.3. Analysis of the Influence of Vertical-Support Damping of the Floating Slab on Vehicle-Track Dynamics Characteristics. To clearly investigate the influence of vertical-support damping of the floating slab (vertical damping of the vibration isolator) on the vehicle-track dynamics, no side-mounted isolator was provided during the analysis, the

(a) (b)

Figure 16: Structure of the side-mounted isolator between adjacent prefabricated steel-spring floating slabs. (a) Top view of the side-mounted isolator. (b) Side view of the side-mounted isolator.

Table 14: Comparison of rail displacement of the floating-slab-track bed.

Calculation working condition	Vertical displacement of the rail (mm)				Lateral displacement of the rail (mm)			
	$L = 3.6$ m		$L = 4.8$ m		$L = 3.6$ m		$L = 4.8$ m	
	−	+	−	+	−	+	−	+
Straight line-140	5.031	2.546	4.002	2.454	0.519	0.209	0.322	0.253
Straight line-160	5.102	2.582	4.173	2.471	0.523	0.218	0.329	0.263
Straight line-200	5.331	2.683	4.446	2.540	0.745	0.375	0.588	0.356
Curve-140	5.316	2.670	4.305	2.603	0.624	0.292	0.397	0.320
Curve-160	5.340	2.698	4.307	2.601	0.787	0.286	0.385	0.303
Maximum change (%)	49.77		40.78		63.66		39.45	

L: length; −: side-mounted isolators are not installed; +: side-mounted isolators are installed.

Table 15: Comparison of displacement of the floating-slab-track bed.

Calculation working condition	Vertical displacement of the floating slab (mm)				Lateral displacement of the floating slab (mm)			
	$L = 3.6$ m		$L = 4.8$ m		$L = 3.6$ m		$L = 4.8$ m	
	−	+	−	+	−	+	−	+
Straight line-140	3.741	2.016	2.995	1.849	0.252	0.104	0.127	0.118
Straight line-160	3.759	2.033	3.006	1.850	0.347	0.111	0.196	0.125
Straight line-200	3.763	2.039	3.102	1.859	0.503	0.244	0.385	0.217
Curve-140	3.718	1.990	2.864	1.772	0.152	0.145	0.289	0.195
Curve-160	3.726	1.999	2.975	1.789	0.241	0.103	0.241	0.170
Maximum change (%)	46.48		40.07		68.01		43.64	

L: length; −: side-mounted isolators are not installed; +: side-mounted isolators are installed.

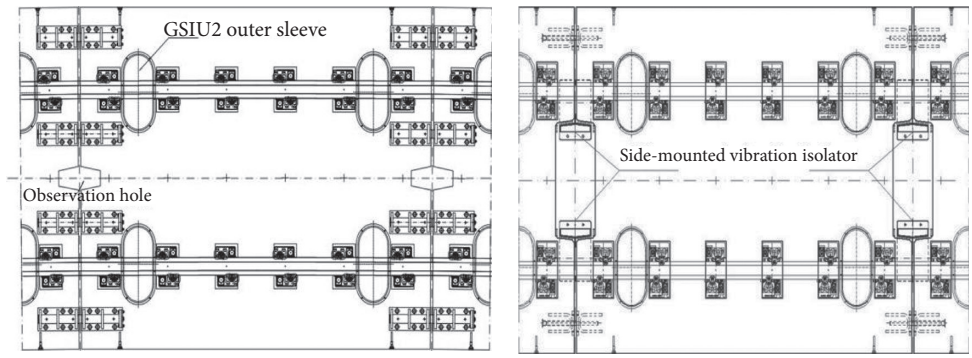

(a) (b)

Figure 17: Prefabricated 3.6 m steel-spring floating-slab track. (a) Slab without side isolators. (b) Slab with side isolators.

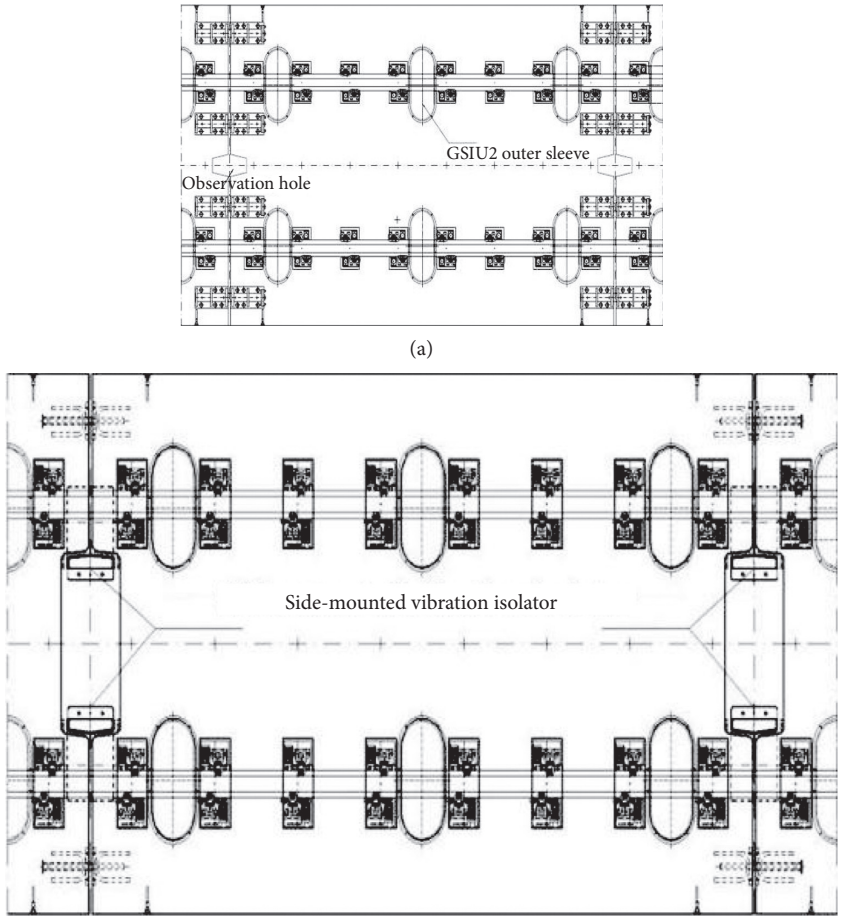

Figure 18: Prefabricated 4.8 m steel-spring floating-slab track. (a) Slab without side isolators. (b) Slab with side isolators.

vertical-damping range of the isolator (Figure 8) was set in the range of 0–100 kN·s/m, and other parameters were left unchanged. For the five working conditions under consideration, we calculated the dynamic response of the intercity EMU train running on the 3.6 m and 4.8 m prefabricated steel-spring floating-slab-track beds.

Figures 14 and 15 prove the following:

(i) The vertical acceleration of the car body (Figure 12) and the vertical force between the wheel and rail are reduced with the increase of the vertical damping of the isolator, which can also improve the vertical dynamic performance of the vehicle. For the 3.6 m or 4.8 m long floating slab, when the vertical damping values are >20 and >50 kN·s/m, respectively, the vertical force between the wheel and rail and the vertical acceleration of the car body are not obvious.

(ii) An increase in vertical damping by the vibration isolator led to a decrease in the vertical displacement of the floating slab (Figure 13), the vertical acceleration of the floating slab, and the vertical displacement of the rail. By appropriately increasing the isolator vertical damping, the vertical-displacement vibration response of the floating slab and the rail can be reduced to some extent. The economical and preferred vertical-damping ranges for the 3.6 m and 4.8 m long floating tracks are 10–30 and 40–60 kN·s/m, respectively, based on the vertical-vibration performance of the floating slab and the vertical deformation of the rail.

(iii) Calculation results show that the vertical damping by the vibration isolator is related to the lateral force of the axle, the derailment coefficient, the wheel-load shedding rate, the lateral acceleration of the vehicle body, the lateral stability of the vehicle body, the ride-comfort index, the vertical and lateral acceleration of the rail, the lateral displacement of the rail, the lateral displacement of the floating slab, and the lateral acceleration of the floating slab.

4.4. Analysis of the Influence of the Side-Mounted Isolator on Vehicle-Track Dynamics. It can be seen from the calculation results in Section 4.3 that the amount of vertical displacement of the rail and the floating slab is large under various working conditions. In order to improve the local stiffness of the floating slab end and improve the dynamic performance of the floating-slab-track bed, a side-mounted isolator

Table 16: Comparison of vertical dynamic performance of the train on the floating-slab-track bed.

Calculation working condition	Vertical-vibration acceleration of the car body (g)				Vertical stability of the car body			
	$L = 3.6$ m		$L = 4.8$ m		$L = 3.6$ m		$L = 4.8$ m	
	−	+	−	+	−	+	−	+
Straight line-140	0.048	0.047	0.042	0.042	1.550	1.549	1.563	1.558
Straight line-160	0.055	0.053	0.050	0.048	1.825	1.823	1.829	1.826
Straight line-200	0.059	0.057	0.057	0.053	1.872	1.870	1.872	1.871
Curve-140	0.045	0.045	0.044	0.041	1.620	1.619	1.630	1.626
Curve-160	0.050	0.049	0.046	0.045	1.651	1.649	1.654	1.652
Maximum change (%)	3.64		7.01		0.12		0.32	

L: length; −: side-mounted isolators are not installed; +: side-mounted isolators are installed.

(Figure 16) was added at each end of the floating slab (Tables 14 and 15). We considered the situations without (Figures 17(a) and 18(a)) and with (Figures 17(b) and 18(b)) side-mounted isolators. For the five working conditions (straight lines and curves), the dynamic response of the intercity EMU train running on the 3.6 m and 4.8 m long prefabricated steel-spring floating-slab-track beds was calculated.

Results of the analysis revealed the following:

(i) For the 3.6 m and 4.8 m long prefabricated steel-spring floating-slab-track beds, whether or not the side-mounted isolators are installed, the running-safety index and the ride-comfort index are basically similar during the intercity EMU train operation; it can be concluded that the impact of the side-mounted isolator on vehicle dynamic performance is not significant when the device is installed. Specifically, according to the analysis results, the addition of the side-mounted isolator can notably reduce the vertical force between the wheel and rail and the vertical-vibration acceleration of the vehicle body while slightly reducing the vertical stability of the vehicle body (Table 16). Accordingly, the side-mounted isolator can improve the vertical dynamic performance of the vehicle.

(ii) For the 3.6 m and 4.8 m long steel-spring floating-slab-track beds, after adding the side-mounted vibration isolator, the track deformation and vibration-response index are significantly reduced. That is, side-mounted isolator improves the stability of the floating-slab bed significantly. In particular, the addition of a side-mounted isolator can greatly reduce the vertical dynamic displacement of the floating-slab track. On the basis of the current design of 3.6 m and 4.8 m long prefabricated floating slabs, four side-mounted isolators should be added. Under each working condition, the maximum vertical displacement of the rail is reduced from 5.340 to 2.698 mm and from 4.446 to 2.603 mm, respectively, indicating maximum reductions of ~50% and ~40%. Maximum vertical displacement of the floating slab is reduced from 3.763 to 2.039 mm and from 3.102 to 1.859 mm, respectively, indicating maximum reductions of ~47% and ~40%. Similarly, after the side-mounted isolator is added, the lateral displacement of the rail and floating slab was reduced within 40%–68%.

5. Conclusions

Research shows that prefabricated steel-spring floating-slab track, which is traditionally used for low-speed lines, can actually be used for higher-speed lines and can also achieve significant results for the vibration and noise reduction function under conditions of driving safety and operational stability. The study is an exploratory study of the application of the new prefabricated steel-spring floating-slab track in the field of high-speed rail transportation. From the above analysis, we can draw the following conclusions:

(1) A prefabricated steel-spring floating-slab track can be applied in urban express rail transit systems and can meet the requirements of safety, comfort, and stability of high-speed vehicles while efficiently reducing noise. This is a great guiding principle for the popularization of prefabricated steel-spring floating-slab tracks on high-speed railway lines.

(2) The dynamic performance of the 3.6 m and 4.8 m long prefabricated steel-spring floating slabs is comparable, although the stability of the former is slightly lower than that of the latter. For the shorter length of the prefabricated steel-spring floating-slab track is often used in curved sections, it can be seen that when the short section of the steel-spring floating-slab track is used in curved sections, the stability of the vehicle-track coupled dynamic system will be reduced but will still remain within the acceptable range of the engineering project.

(3) For same-length prefabricated steel-spring floating-slab tracks, as slab thickness increases, the vertical displacement of the rail increases slightly, and lateral stability improves. A change of slab thickness has a little effect on the running-safety and ride-comfort indexes of the intercity EMU train, but the running stability of the vehicle can be slightly improved with increasing thickness of the floating slab. It is shown that the thickness of the track slab has a great effect on the vehicle-track coupled dynamic system; the limit of the thickness of the track slab can achieve

good economic results within the acceptable range of the project.

(4) When the intercity EMU train runs at 140, 160, or 200 km/h in the straight section and at 140 or 160 km/h in the curved section ($R = 1100$ m and $R = 1500$ m) on the 3.6 m or 4.8 m long prefabricated steel-spring floating-slab track, the wheel-axle lateral force, the wheel-rail vertical force, the derailment coefficient, and the wheel-weight reduction rate are each less than the specified code limit value. The lateral and vertical accelerations of the vehicle body are each lower than the specified code limit value. In addition, the stability index is "excellent," and the comfort rating is "comfortable."The analysis results have subverted the previous perception that steel-spring floating-slab track can only be used for low-speed lines. The steel-spring floating-slab track in this project research has achieved very good results and can be promoted as a theoretical basis for the application of floating-slab track for high-speed railway lines.

(5) Appropriately increasing the vertical-support damping of the floating-slab track can improve the vertical dynamic performance of the vehicle, reduce the vertical displacement of the rail, and lower the vibration response of the floating-slab track. We comprehensively considered the dynamic performance of the vehicle and the stability of the track and found that the optimal ranges of vertical damping for the 3.6 m and 4.8 m long prefabricated floating-slab-track isolators are 10–30 and 40–60 kN·s/m, respectively. Choosing the vibration isolator damping in this range can obtain good vibration isolation effect and can save engineering investment.

(6) Adding side-mounted vibration isolators at the joint of the floating slabs can greatly improve the stability of the floating slab and appropriately reduce the vertical vibration response of the vehicle. The invention of the side-mounted vibration isolator is a new exploration to improve the stability of the floating-slab track. Compared with the past, simply increasing the thickness of the track slab to improve the overall quality of the track slab to achieve improved stability, the side-mounted vibrator is undoubtedly economical and effective.

Data Availability

The experimental data used to support the findings of this study are included within the article.

Conflicts of Interest

The authors declare that they have no conflicts of interest.

Acknowledgments

The research was financially supported by the Science and Technology Plan Project of Yuexiu District, Guangzhou—The Urban Express Rail Transit Steel Spring Floating Slab Track System Research (2017-GX-024)—and the Natural Science Foundation of Hunan Province, China (2019JJ40384), which is gratefully acknowledged by the authors.

References

[1] T. R. Xu and C. Z. Geng, "Finite element analysis on natural vibration frequency of floating track structure," *Modern Urban Transit*, vol. 1, pp. 28–33, 2015.

[2] L. Li, T. F. Yin, and Q. Zhu, "Characteristics and energies in different frequency bands of environmental noise in urban elevated rail," *Journal of Traffic and Transportation Engineering*, vol. 18, no. 2, pp. 120–128, 2018.

[3] W. F. Liu and W. N. Liu, "Experimental validation of a numerical model for prediction of metro train-induced ground-surface vibration," *Journal of Vibration Engineering*, vol. 23, no. 4, pp. 373–379, 2010.

[4] T. X. Wu, "On effectiveness of vibration isolation for super-elastic rail support combined with booted sleeper or floating slab track," *Journal of Vibration Engineering*, vol. 20, no. 5, pp. 489–493, 2007.

[5] F. Cui and C. H. Chew, "The effectiveness of floating slab track system—part I. receptance methods," *Applied Acoustics*, vol. 61, no. 4, pp. 441–453, 2000.

[6] D. Chew, "Effectiveness of the floating slab track system constructed at Konya light rail," *Measurement*, vol. 89, pp. 48–54, 2016.

[7] W. Zhai, K. Wang, and C. Cai, "Fundamentals of vehicle-track coupled dynamics," *Vehicle System Dynamics*, vol. 47, no. 11, pp. 1349–1376, 2009.

[8] W. Zhai, P. Xu, and K. Wei, "Analysis of vibration reduction characteristics and applicability of steel-spring floating-slab track," *Journal of Modern Transportation*, vol. 19, no. 4, pp. 215–222, 2011.

[9] M. F. M. Hussein and H. E. M. Hunt, "A numerical model for calculating vibration due to a harmonic moving load on a floating-slab track with discontinuous slabs in an underground railway tunnel," *Journal of Sound and Vibration*, vol. 321, no. 1-2, pp. 363–374, 2009.

[10] G. Lombaert, "The control of ground-borne vibrations from railway traffic by means of continuous floating slabs," *Journal of Sound and Vibration*, vol. 297, pp. 946–961, 2016.

[11] H. E. M. Hunt, "Modelling of rail vehicles and track for calculation of ground-vibration transmission into buildings," *Journal of Sound and Vibration*, vol. 193, no. 1, pp. 185–194, 1996.

[12] L. Xu, J. Zhai, and J. M. Gao, "A probabilistic model for track random irregularities in vehicle/track coupled dynamics," *Applied Mathematical Modelling*, vol. 51, pp. 145–158, 2017.

[13] L. Xu, W. Zhai, and J. Gao, "Extended applications of track irregularity probabilistic model and vehicle-slab track coupled model on dynamics of railway systems," *Vehicle System Dynamics*, vol. 55, no. 11, pp. 1686–1706, 2017.

[14] S. L. Wang, J. Z. Liu, and W. L. Hu, "Study on dynamic characteristics of train-steel," *Spring Floating-Slab Track Interactions, Open Journal of Transportation Technologies*, vol. 8, no. 1, pp. 63–72, 2019.

[15] K. Huang, D. W. Bai, and Y. L. Li, "Coupling dynamic analysis of floating slab track in the urban rail transit," *Applied Mechanics and Materials*, vol. 253–255, pp. 2047–2051, 2012.

[16] L. Ling, X. Li, and J. Yin, "Vibration characteristics of damping pad floating slab on the long-span steel truss cable-stayed bridge in urban rail transit," *Engineering Structures*, vol. 191, pp. 92–103, 2019.

[17] C. X. Lu, J. Shi, and Q. Y. Duan, "Dynamic interaction between metro vehicle and steel spring floating slab track under emergency braking condition," *Journal of Traffic and Transportation Engineering*, vol. 19, no. 1, pp. 96–107, 2019.
[18] S. G. Park, C. K. Chun, G. S. Lee, and S. Y. Jang, "The development of a floating slab track to isolation system," *Transactions of the Korean Society for Noise and Vibration Engineering*, vol. 23, no. 2, pp. 112–122, 2013.
[19] S. Zhu, J. Yang, H. Yan, L. Zhang, and C. Cai, "Low-frequency vibration control of floating slab tracks using dynamic vibration absorbers," *Vehicle System Dynamics*, vol. 53, no. 9, pp. 1296–1314, 2015.
[20] D.-Y. Ding, W.-N. Liu, K.-F. Li, X.-J. Sun, and W.-F. Liu, "Low frequency vibration tests on a floating slab track in an underground laboratory," *Journal of Zhejiang University-Science A*, vol. 12, no. 5, pp. 345–359, 2011.
[21] C. D. Jiang and X. Y. Lei, "Analysis of the dynamic properties of urban rail transit steel spring floating slab," *Modern Urban Transit*, vol. 3, pp. 34–41, 2013.
[22] J. C. Wei, P. He, and Y. J. Li, "Analysis on the vibration attenuation of metro steel spring floating slab track," *China Railway Science*, vol. 33, pp. 17–25, 2012.
[23] W. M. Zhai, *Vehicle-track Coupled Dynamics*, Science Press, Beijing, China, 2015, in Chinese.
[24] X. Xiao, X. Jin, Y. Deng, and Z. Zhou, "Effect of curved track support failure on vehicle derailment," *Vehicle System Dynamics*, vol. 46, no. 11, pp. 1029–1059, 2008.
[25] W. M. Zhai and H. Xia, *Train-track-bridge Dynamic Interaction: Theory and Engineering Application*, Science Press, Beijing, China, 2011.
[26] L. Ling, X.-B. Xiao, J.-Y. Xiong, Z.-F. Wen, and X.-S. Jin, "Erratum to: a 3D model for coupling dynamics analysis of high-speed train/track system," *Journal of Zhejiang University-Science A*, vol. 16, no. 2, p. 170, 2015.
[27] L. Ling, Q. Zhang, X. Xiao, Z. Wen, and X. Jin, "Integration of car-body flexibility into train–track coupling system dynamics analysis," *Vehicle System Dynamics*, vol. 56, no. 4, pp. 485–505, 2017.
[28] L. Ling, X.-S. Xiao, and X. S. Jin, "Development of a simulation model for dynamic derailment analysis of high-speed trains," *Acta Mechanica Sinica*, vol. 30, no. 6, pp. 860–875, 2014.
[29] W. N. Liu, D. Y. Ding, and K. F. Li, "Experimental study of the low-frequency vibration characteristics of steel spring floating slab track," *China Civil Engineering Journal*, vol. 44, no. 8, pp. 118–125, 2011, in Chinese.
[30] K. Wei, Y. L. Dou, and Q. L. Yang, "Random vibration analysis and parameter optimization of steel-spring floating-slab track," *Journal of Huazhong University of Science and Technology(Natural Science Edition)*, vol. 45, no. 8, pp. 115–119, 2017.
[31] W.-M. Zhai, "Two simple fast integration methods for large-scale dynamic problems in engineering," *International Journal for Numerical Methods in Engineering*, vol. 39, no. 24, pp. 4199–4214, 1996.
[32] GB/T5599-1985, *Railway Vehicles-Specification for Evaluation the Dynamic Performance and Accreditation Test*, China Communication Press, Beijing, China, 1985.
[33] TB/T2360-1993, *Identification Method and Evaluation Criteria for Railway Locomotive Dynamic Performance Test*, China Communication Press, Beijing, China, 1993.